Compact Switched-Beam Array Antenna with a Butler Matrix and a Folded Ground Structure

Young-Jun Kim, Ye-Bon Kim, Hyun-Jun Dong, Yong Soo Cho 🆔 **and Han Lim Lee *** 🆔

School of Electrical and Electronics Engineering, Chung-Ang University, 84 Heukseok-ro, Dongjak-gu, Seoul 06974, Korea; yhjkim747@cau.ac.kr (Y.-J.K.); equa1ity@cau.ac.kr (Y.-B.K.); honestdong87@cau.ac.kr (H.-J.D.); yscho@cau.ac.kr (Y.S.C.)

* Correspondence: hanlimlee@cau.ac.kr; Tel.: +82-2-820-5298

Abstract: A compact switched-beam array antenna, based on a switched Butler matrix with four folded ground antennas, is presented for unmanned aerial vehicle (UAV) applications. The folded ground structure, including a slotted patch radiator surrounded by multiple air-gapped ground layers, is adopted to maximize compactness. The extra ground layers provide extra capacitive coupling around the patch antenna, resulting in a down-shift of resonant frequency and a reduction in the antenna size. Also, to optimize aerial operation with a wider beam coverage, the 1×4 array is integrated with a switched Butler matrix controlled by a microcontroller unit (MCU). The choice of the Butler matrix reduces the complexity of beamforming circuitry and avoids the use of high-cost phase shifters requiring extra control-bit signals. Further, the array antenna is optimized for high isolation among the antenna ports and a minimal UAV body effect. Then, the proposed structure was verified at 1.96 GHz for test purposes only, and the array size, excluding the antenna case, was $2.16\lambda_o \times 0.54\lambda_o \times 0.07\lambda_o$. The measured 10 dB impedance bandwidth for all antenna elements in the array was always better than 3.4%, and the isolation among the antenna ports was also better than 19 dB. The measured peak gain, excluding the loss of the switched Butler module, was about 9.98 dBi, on average. Lastly, the measured peak scan angles were observed at $-39°$, $-17°$, $9°$ and $31°$ according to switching modes.

Keywords: compact antenna; folded ground antenna array; switched-beam array; switched Butler matrix; UAV-mounted antenna

---

1. Introduction

In recent years, unmanned aerial vehicles (UAVs) have played a critical role in various technical fields, such as warfare systems, security and surveillance, structural health monitoring, unmanned delivery, agricultural applications, and communication applications [1–5]. Typically, drones have been used widely more than ever in a variety of industries, with the increasing demand for drone-based sensors and radars, drone-based aerial base stations, autonomous drones for emergency response, and so on [6–10]. Since UAV applications, including drones, require a compact antenna system due to their weight limit, an optimal antenna structure for UAVs must be studied. Moreover, a flexible beam coverage is required to further maximize the aerial mobility and flying time of UAVs. As shown in Figure 1, the modern UAV applications need multiple-device communication for controllers, infrastructures, base stations, vehicles, and/or various portable electronics. To ensure highly reliable UAV-to-ground communication, a beamforming technique must be used. This is because the use of a single omnidirectional antenna is susceptible to interferences from neighboring devices and a lack of gain in the long distance from the air to the ground. Further, since the antenna line-of-sight (LoS) keeps changing due to the three-dimensional mobility of UAVs, a beam-steering operation is required to maintain reliable communication channels.

That is, a compact array antenna for beamforming is required for future UAV applications. The array structures using conventional radiation elements like monopole, dipole, or patch antennas suffer from large size, including ground planes, and struggle to satisfy sufficient radiation efficiency and high directivity. Previously, there has been a lot of research into the realization of a compact antenna, including techniques such as inverted planar structures [11–13], dielectric resonators [14], simple patch antennas with reflectors [15–19] and shorting-pin structures [20,21]. However, these techniques require the direct manipulation of radiating elements, and thus the optimization of the beam patterns becomes difficult with respect to the UAV body effect. To overcome the issues of the antenna size and the UAV body effect, a folded ground element [22] can be effectively used. The folded ground structure can adjust operation frequency and antenna gain through the air-gapped ground elements, without modifying the radiation element. Further, the UAV body effect on the antenna radiation can be mitigated because the radiation patch is geometrically shielded by three-dimensional folded ground layers, consisting of side ground walls and topped elements.
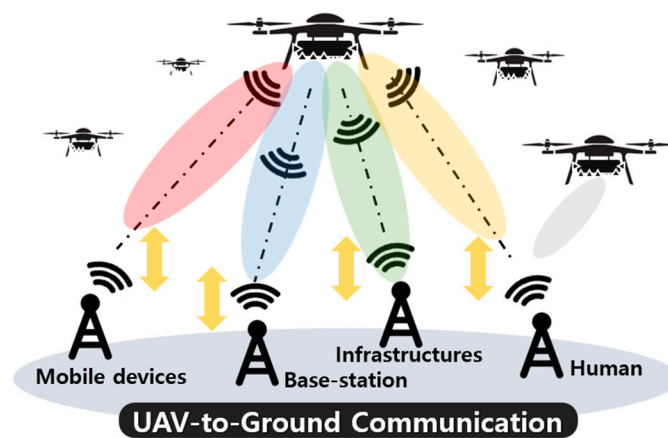

Figure 1. An efficient antenna module required for various unmanned aerial vehicle (UAV)-to-ground communication.

In addition to the compactness of the antenna, a flexible control for the radiation patterns must also be supported. Although the conventional phased array architecture can perform well in beam steering, expensive phase shifters with multiple control bits are required. Instead, previous research suggested the use of antennas with PIN diodes [23–25], but the beam-steering capability is insufficient for UAV applications. Thus, to effectively reconfigure beam patterns, the Butler matrix can be a good candidate since the limited scan angles can be compensated by the aerial mobility of UAVs. Moreover, effective uses of the Butler matrix have been demonstrated in mmWave and 5G applications [26–29]. Therefore, in this paper, a new array architecture based on folded ground structures for UAV applications is presented. Although the concept of a folded ground element has been previously proposed [22], the extension of the folded ground structures to the array has not yet been studied. Further, the integration of the folded ground array structure with a switched-beam network such as the Butler matrix has not been investigated at all. To prove the feasibility of the folded ground structures for UAV applications, the array architecture must be verified because element-to-element isolation, return loss variation and realized array antenna gain for multiple beams at different angles play critical roles in real performance. Therefore, a 1×4 switched beamforming antenna module, based on the folded ground array structure, is presented with the help of a switched Butler matrix and a microcontroller unit (MCU) in this article for the first time.

2. Design of the Proposed Structure

Figure 2a shows the proposed 1 × 4 module, including the switched-beam network and the folded ground array antenna. The switched-beam generator is configured by an RF switch-integrated 4 × 4 Butler matrix, an MCU and a portable battery for test purposes. Then, the 4 × 4 Butler matrix outputs are connected to the proposed folded ground array, which can produce four different beams.
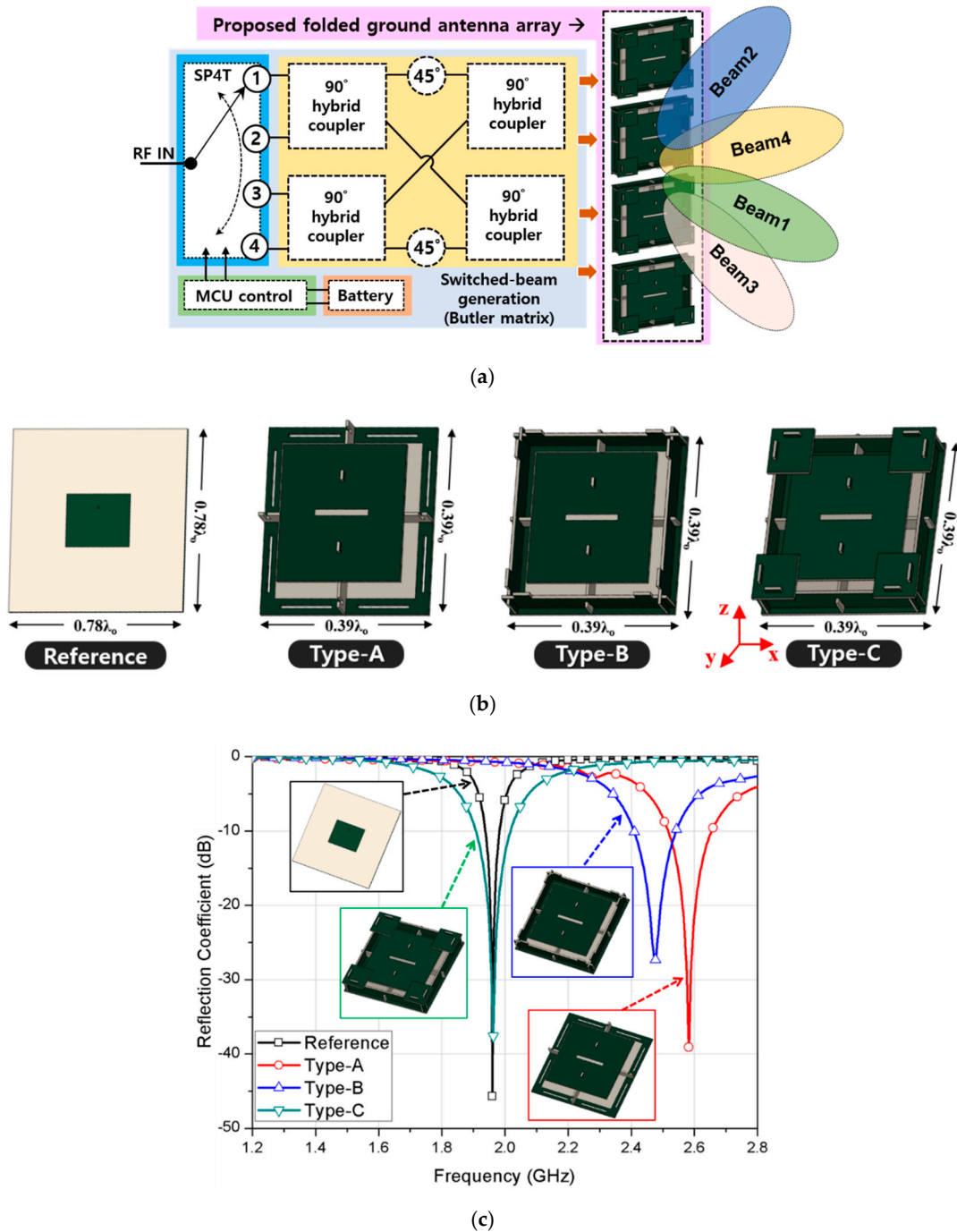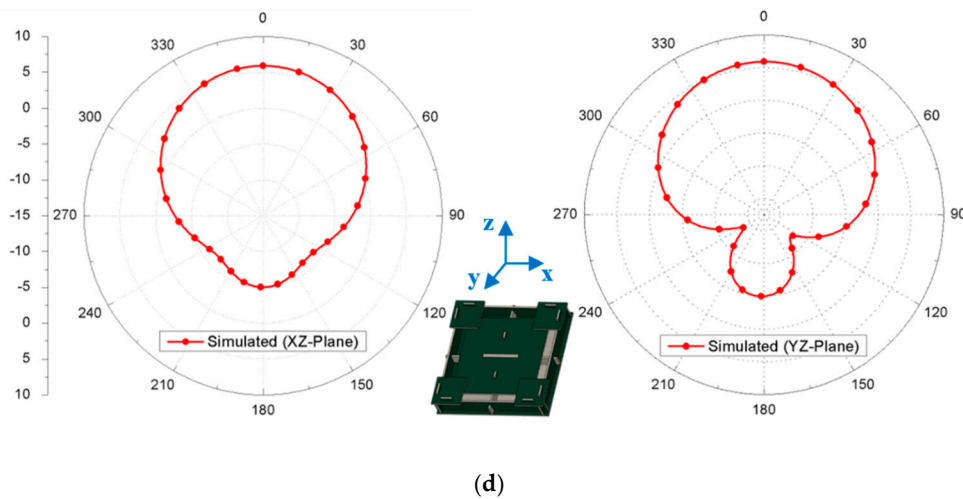

(a)

(b)

(c)

Figure 2. *Cont.*

(**d**)

Figure 2. (**a**) A block diagram of the overall switched-beam module, (**b**) the antenna element description (the conventional patch as a reference, a slotted patch as type-A, a slotted patch with side ground walls as type-B, a slotted patch with a folded ground as type-C), (**c**) the simulated reflection coefficients for each type, and (**d**) radiation patterns in xz- and yz-planes.

Figure 2b shows the conventional patch, a slotted patch, a slotted patch with side ground walls, and a proposed slotted patch with a folded ground. Here, FR4 substrate with a relative permittivity of 4.3, a loss tangent of 0.018 and a thickness of 1 mm is used for all antenna simulations. The conventional patch is designed at 1.96 GHz as a reference in order to compare the size and electrical performance of the proposed structure. To ensure sufficient radiation efficiency and gain, the ground size for the conventional patch was set to $0.78\ \lambda_o \times 0.78\ \lambda_o$, whereas the other types in Figure 2 have an identical size of $0.39\ \lambda_o \times 0.39\ \lambda_o \times 0.07\ \lambda_o$ at 1.96 GHz. Although the height of the proposed structure increases, the overall volume ratio becomes smaller due to the relatively large reduction in width and length of the required ground plane. Figure 2c shows the center frequencies of type-A, type-B and type-C, as well as the reference patch antenna. The detailed design information for a single folded ground element can be found in [22]. The designed single slotted patch with a folded ground shows a simulated 10 dB impedance bandwidth of 5.6% and a simulated peak gain of 6.1 dBi. Further, to verify the array performance of the folded ground structure, four slotted patches with folded ground structures are integrated as shown in Figure 3a,b. The total array volume is optimized to $2.16\ \lambda_o \times 0.54\ \lambda_o \times 0.07\ \lambda_o$ at 1.96 GHz, excluding RF connectors. Each input port is equally spaced by $0.56\ \lambda_o$ to reduce the coupling effect among the ports. Figure 3c shows the simulated reflection coefficients of the folded ground array. The 10 dB impedance bandwidth for each antenna element in the array shows approximately 3.2%, slightly narrower than the single antenna case, due to the coupling effect in the array. Also, the simulated isolation characteristics among the four ports are shown in Figure 3d, where the isolation is always better than 17.8 dB within the 10 dB impedance bandwidth.
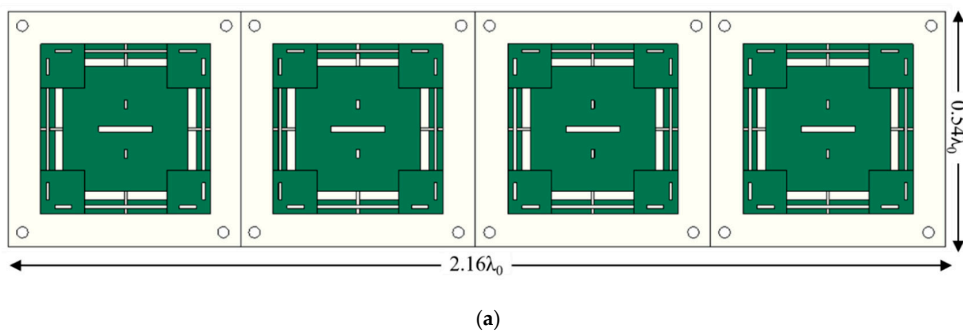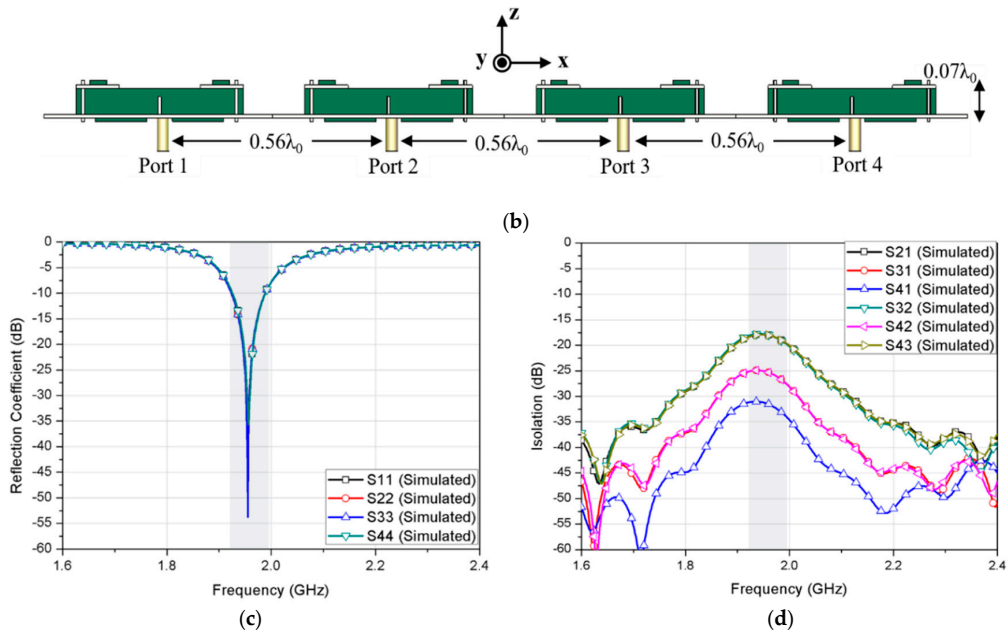

(**a**)

Figure 3. *Cont.*

Figure 3. Proposed array antenna with (**a**) a top-view and (**b**) a side-view, as well as the simulated S-parameters of each input port for (**c**) the reflection coefficient and (**d**) the isolation characteristic.

Since the beamforming performance of the proposed array is to be driven by a 4×4 Butler matrix, the radiation patterns according to the ideal Butler matrix output phases are also simulated at 1.96 GHz. The peak gains are better than 10.9 dBi, and the four peak angles are observed at $\pm 12°$ and $\pm 38°$ with a half power beamwidth (HPBW) between $23°$ and $27°$.

3. Measured Results

To verify the proposed structure, a single folded ground antenna was first constructed with the same FR4 substrate used in the simulation. The picture of the fabricated antenna, measured reflection coefficients and radiation patterns with the simulated results are shown in Figure 4. The measured results showed a good agreement with the simulated results.
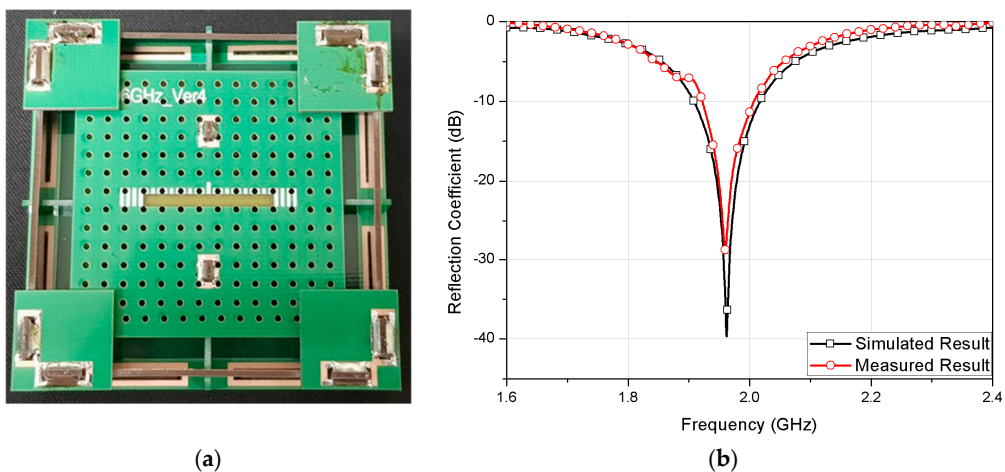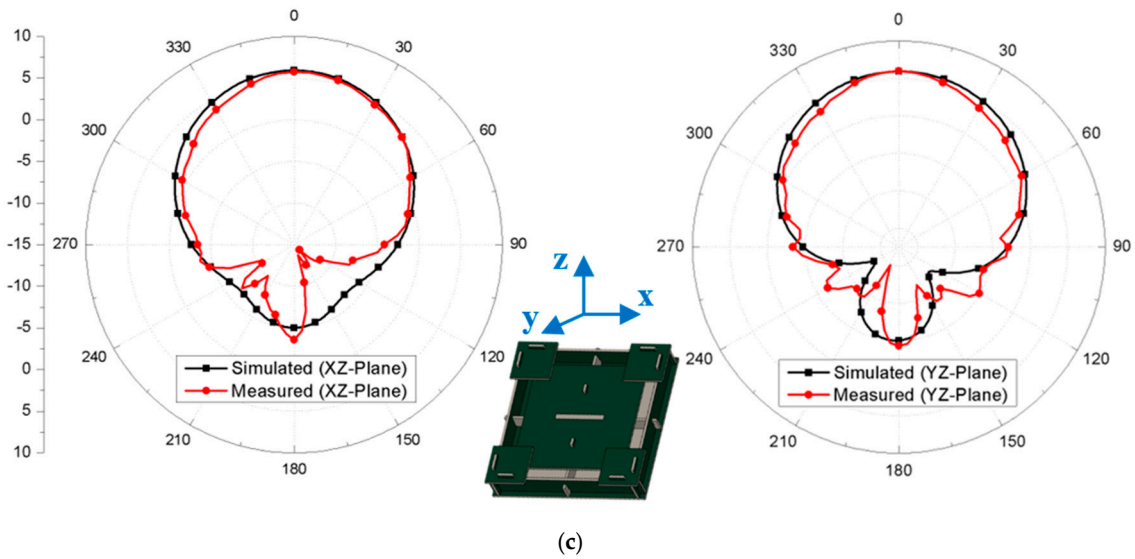

Figure 4. *Cont.*

(**c**)

Figure 4. (**a**) The fabricated single antenna, and the measured (**b**) reflection coefficients and (**c**) radiation patterns in xz- and yz-planes.

Further, the 1 × 4 array antenna module was implemented with a switched Butler matrix. The switched Butler matrix is configured by a single-pole-four-throw (SP4T) RF switch, four single-pole-double-throw (SP2T) RF switches connecting to external 50 Ω terminations, and four LTCC-based quadrature hybrid couplers, as shown in Figure 5a. The measured path losses and phases are also shown in Figure 5b–i. The maximum path loss including RF switches was about 1.9 dB. The measured magnitude balances for all operation modes were found to be approximately 0.6 ± 0.5 dB, showing a reasonable consistency.
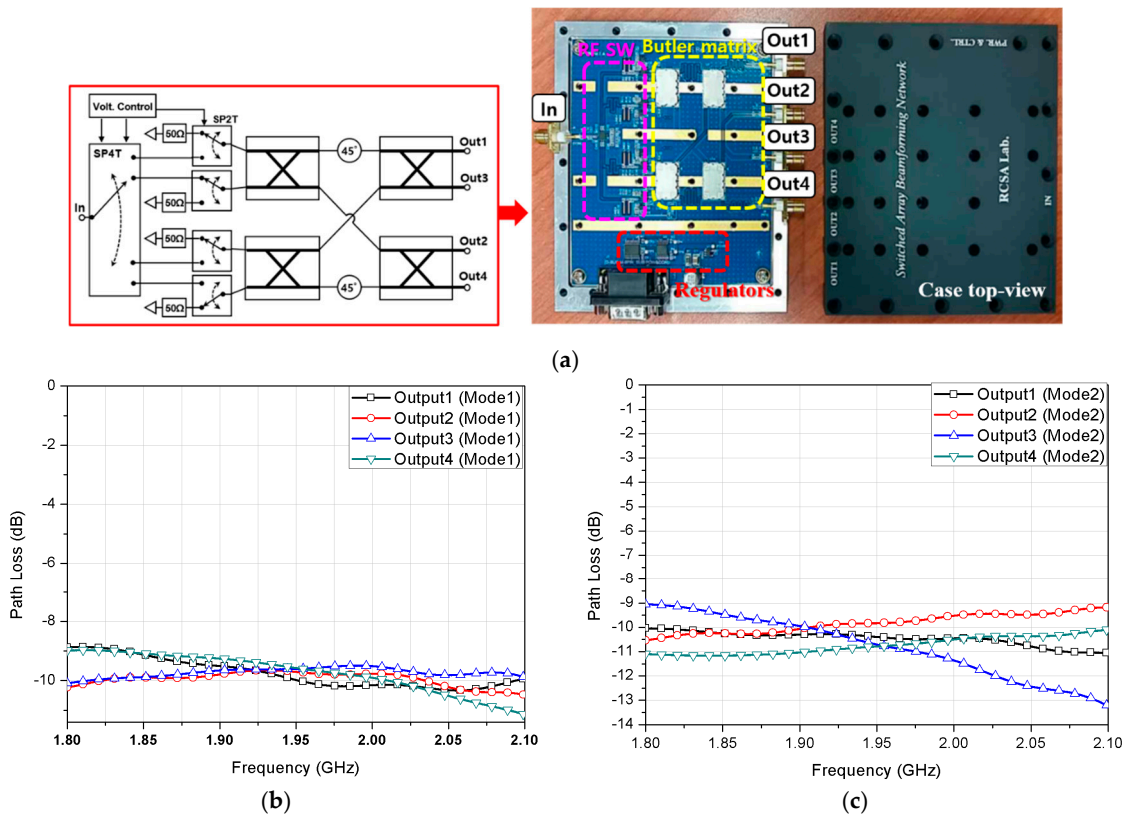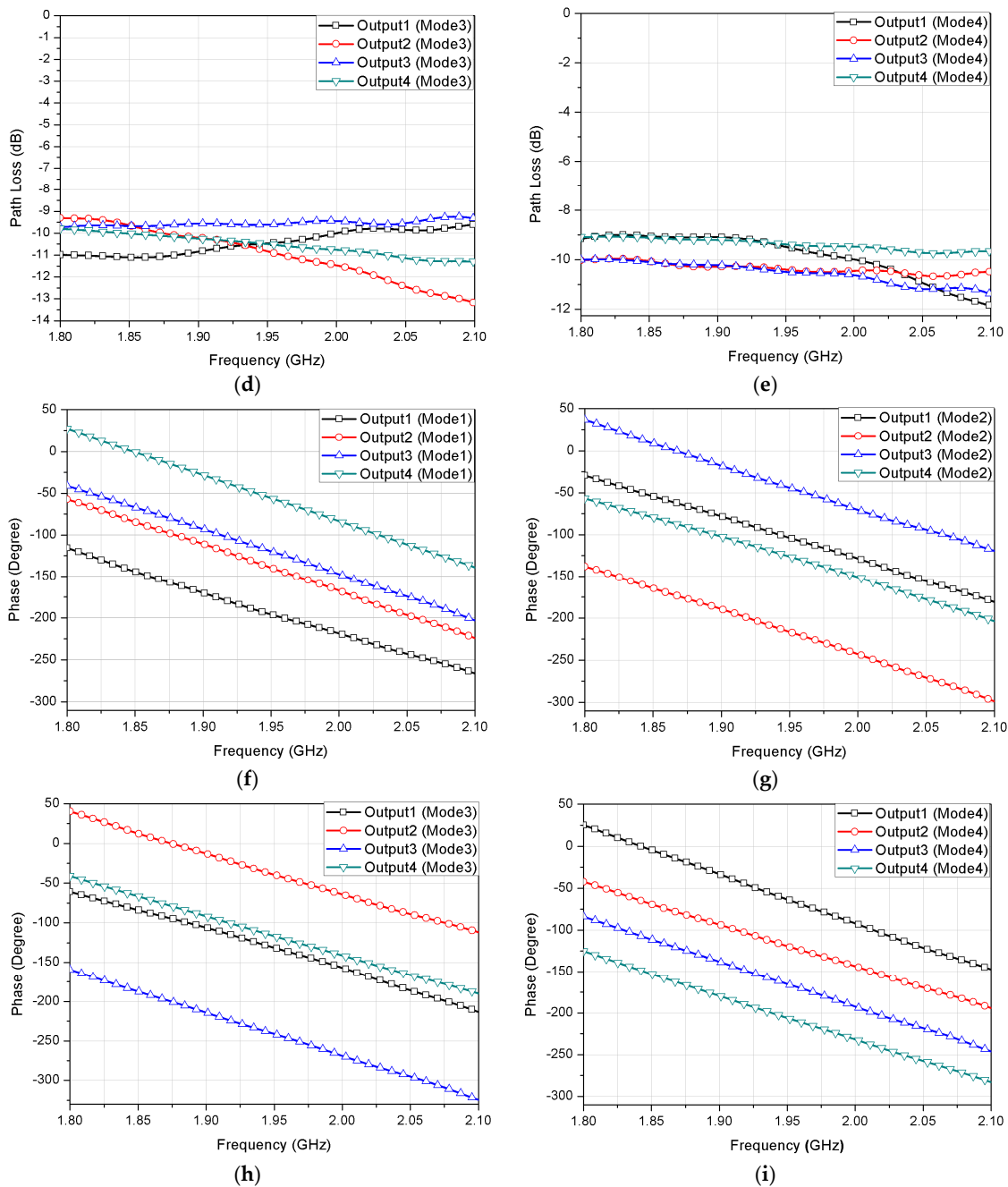

(**a**)

(**b**)

(**c**)

Figure 5. *Cont.*

Figure 5. (**a**) Implementation of the 1 × 4 switched Butler matrix, and (**b**–**i**) the measured magnitude and phase performance.

However, the measured phase balance showed a maximum deviation of 43° at mode 3 compared to an ideal phase balance. Further, the best phase balance was observed at mode 4, where all ports were phase-matched to the ideal values with a deviation of less than 11°. The comparison results are summarized in Table 1, where the ideal phases are rescaled according to the measured phases of output 1 at each mode.

Table 1. Comparison between the measured and ideal magnitudes and phases at 1.96 GHz.

Mode		Output1		Output2		Output3		Output4	
		Measured	Ideal	Measured	Ideal	Measured	Ideal	Measured	Ideal
MAG (dB)	1	−10.0	−9	−9.7	−9	−9.5	−9	−9.6	−9
	2	−10.4	−9	−9.8	−9	−10.8	−9	−10.7	−9
	3	−10.4	−9	−10.9	−9	−9.5	−9	−10.5	−9
	4	−9.6	−9	−10.4	−9	−10.5	−9	−9.4	−9
PH (°)	1	159	159	−145	−156	−125	−111	−61	−66
	2	−109	−109	138	116	−49	−19	−131	−154
	3	−136	−136	−44	−1	114	134	−122	−91
	4	−69	−69	−124	−114	−170	−159	149	156

Lastly, Figure 6a shows the implementation of the proposed array antenna with a shield case to reduce the coupling effect among the antenna ports as well as the UAV body.
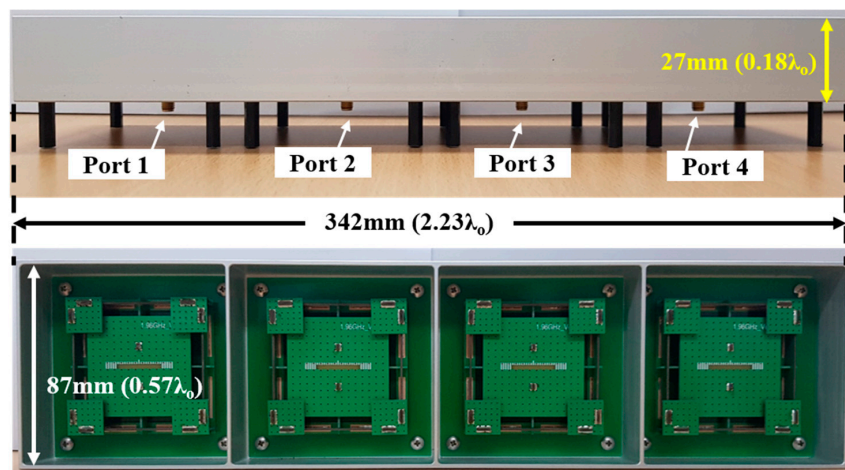
(**a**)
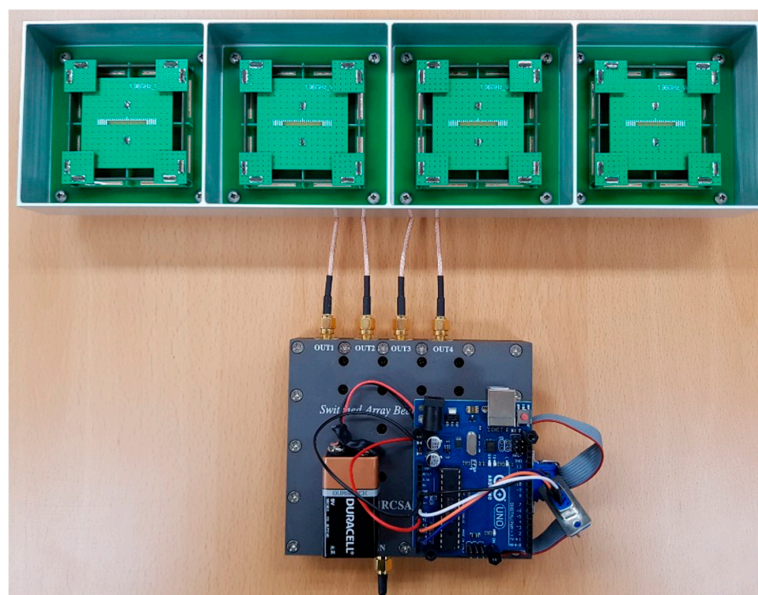
(**b**)

Figure 6. Implementation of (**a**) the proposed folded ground array antenna and (**b**) the overall module.

Further, the overall array antenna module including the switched Butler matrix is shown in Figure 6b. It is noted that the switched Butler matrix and MCU controller can be integrated into the mainboard of the UAV internally. To see the pure reflection coefficient and isolation characteristics of the proposed array antenna, the return losses and port-to-port isolation of Figure 6a were first measured as shown in Figure 7. Here, the measured 10 dB impedance bandwidth varied from 3.4% to 4.5% for each port. Also, the measured isolation magnitudes among the ports were always better than 19 dB within the measured 10 dB impedance bandwidth, showing a good agreement with the simulation.
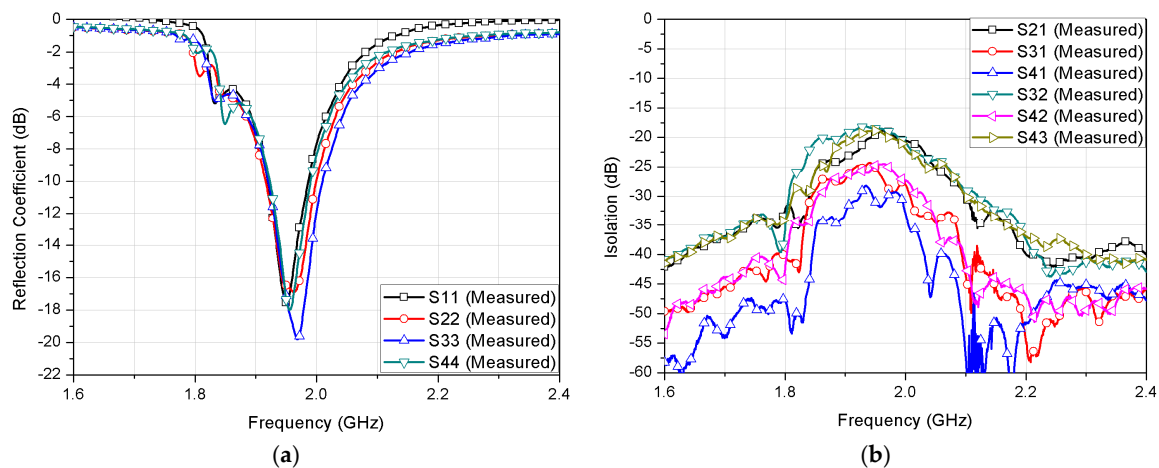

Figure 7. The measured (**a**) reflection coefficients and (**b**) isolation magnitudes for all ports of the proposed array antenna.

Since there was a mismatch in the magnitude and phase balance between the fabricated and ideal switched Butler matrices, the proposed array antenna was re-simulated according to the measured magnitude and phases for all modes. Thus, an accurate comparison between the measured radiation patterns driven by the actual Butler matrix and the simulated radiation patterns could be made as shown in Figure 8. Here, it should be noted that the measured radiation pattern included the loss of the switched Butler matrix, and thus the measured antenna gain seemed to be lower compared with the simulated results. The simulation with the ideal Butler matrix showed an average peak gain of 11.2 dBi with the peak angles at ±12° and ±38°, and the maximum side lobe of −10 dB. Also, the simulated results for the fabricated Butler matrix showed an average peak gain of 10.97 dBi, and the peak angles were located at 13°, −36°, 38° and −12° corresponding to beams 1, 2, 3 and 4, respectively. Moreover, the simulated side lobes for beams 1, 2, 3 and 4 were −12.2, −6.8, −4.2 and −13.3 dB, respectively. Comparing the two simulated cases in Figure 8, the imbalance in the magnitudes and phases of the Butler matrix caused an increase in the side lobe levels, while the peak angles remained very similar. Further, the measured average peak gain including the insertion loss of 4.1 dB due to the switched Butler network was about 5.88 dBi. That is, the pure peak gain of the proposed array antenna would only be 9.98 dBi on average. Lastly, the measured peak angles were at 9°, −39°, 31° and −17°, corresponding to beams 1, 2, 3 and 4, respectively, and the maximum side lobe was about −4 dB for beam 3 due to the worst imbalance of the realized Butler matrix. Nevertheless, the measured antenna module showed a good agreement with the simulated switched-beam performances.
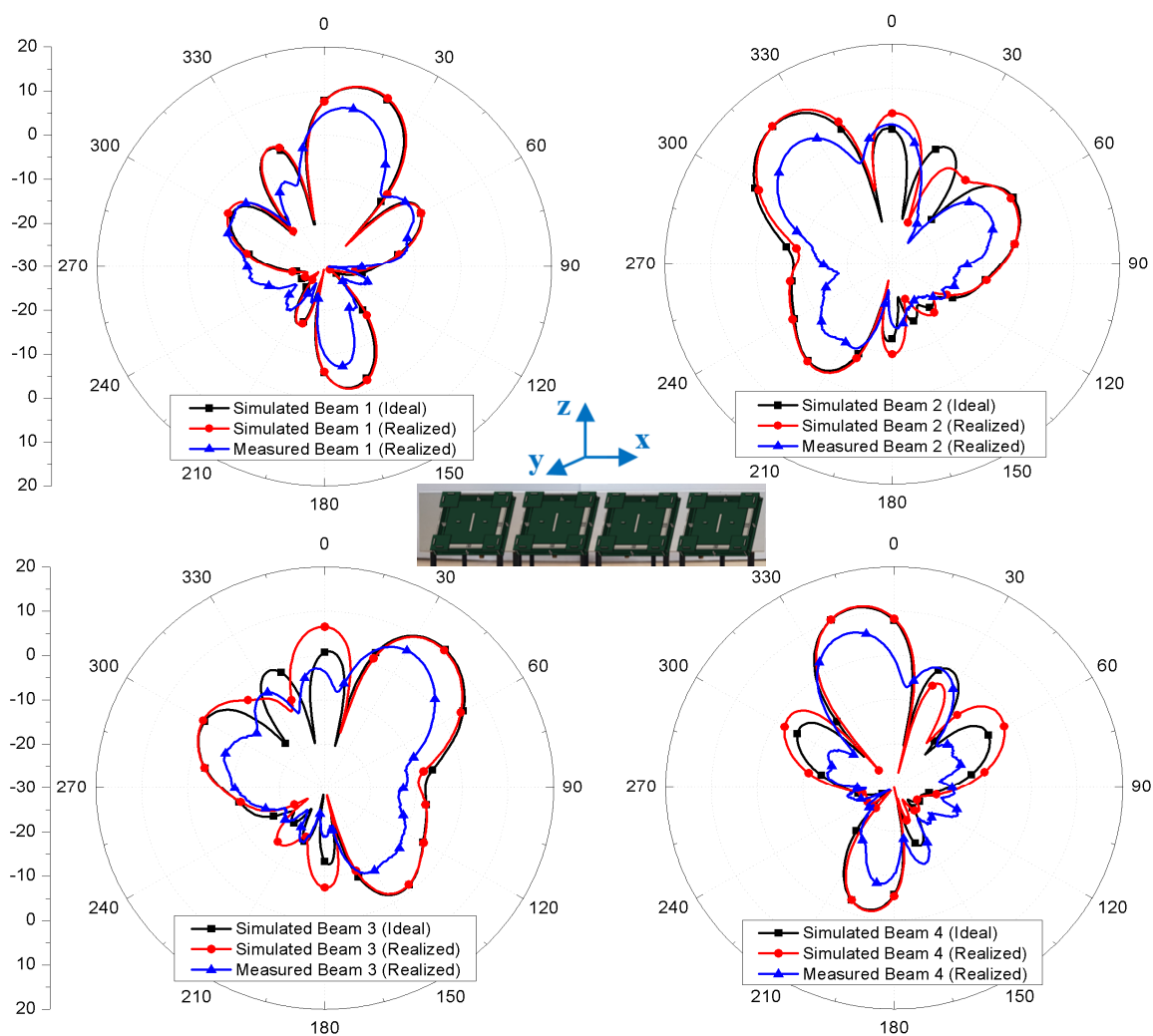
Figure 8. The simulated and measured radiation patterns in the xz-plane for the switched beams.

4. Conclusions

Due to the increasing demand for the use of UAVs in many applications, a compact antenna with an efficient beamforming capability is needed more than ever. Thus, in this article, a new compact antenna module using a folded ground array structure was designed and verified at a test frequency of 1.96 GHz. The fabricated volume of the proposed array, excluding the shield case, was about $2.16 \, \lambda_o \times 0.54 \, \lambda_o \times 0.07 \, \lambda_o$. The measured 10 dB impedance bandwidths for all the antenna elements were better than 3.4%, and the isolation among the four antenna ports was always better than 19 dB. The measured average peak gain, excluding the loss of the switched Butler network, was approximately 9.98 dBi. Further, the measured peak scan angles were about −39°, −17°, 9° and 31° according to the switching operation of the Butler matrix, showing a good agreement with the simulated results.

Conflicts of Interest: The authors declare no conflict of interest.

References

1. Grimaccia, F.; Bonfante, F.; Battipede, M.; Maggiore, P.; Filippone, E. Risk Analysis of the Future Implementation of a Safety Management System for Multiple RPAS Based on First Demonstration Flights. *Electronics* **2017**, *6*, 50. [CrossRef]
2. Wan, P.; Hao, B.; Li, Z.; Ma, X.; Zhao, Y. Accurate Estimation the Scanning Cycle of the Reconnaissance Radar Based on a Single Unmanned Aerial Vehicle. *IEEE Access* **2017**, *5*, 22871–22879. [CrossRef]
3. Baek, H.; Lim, J. Design of Future UAV-Relay Tactical Data Link for Reliable UAV Control and Situational Awareness. *IEEE Commun. Mag.* **2018**, *56*, 144–150. [CrossRef]
4. Kim, S.J.; Cho, J.; Cote, M.J. Drone-Aided Healthcare Services for Patients with Chronic Diseases in Rural Areas. *J. Intell. Robot. Syst.* **2017**, *88*, 163–180. [CrossRef]
5. Mitcheson, P.D.; Boyle, D.; Kkelis, G.; Yates, D.; Saenz, J.A.; Aldhaher, S.; Yeatman, E. Energy-Autonomous Sensing Systems Using Drones. In Proceedings of the 2017 IEEE Sensors, Glasgow, UK, 29 October–1 November 2017.
6. Ullah, H.; Nair, N.G.; Moore, A.; Nugent, C.; Muschamp, P.; Cuevas, M. 5G Communication: An Overview of Vehicle-to-Everything, Drones, and Healthcare Use-Cases. *IEEE Access* **2019**, *7*, 37251–37268. [CrossRef]
7. Kovalchukov, R.; Moltchanov, D.; Samuylov, A.; Ometov, A.; Andreev, S.; Koucheryavy, Y.; Samouylov, K. Analyzing Effects of Directionality and Random Heights in Drone-Based mmWave Communication. *IEEE Trans. Veh. Technol.* **2018**, *67*, 10064–10069. [CrossRef]
8. Naqvi, S.A.R.; Hassan, S.A.; Pervaiz, H.; Ni, Q. Drone-Aided Communication as a Key Enabler for 5G and Resilient Public Safety Networks. *IEEE Commun. Mag.* **2018**, *56*, 36–42. [CrossRef]
9. Fotouhi, A.; Ding, M.; Hassan, M. Flying Drone Base Stations for Macro Hotspots. *IEEE Access* **2018**, *6*, 19530–19539. [CrossRef]
10. Hildmann, H.; Kovacs, E. Review: Using Unmanned Aerial Vehicles (UAVs) as Mobile Sensing Platforms (MSPs) for Disaster Response, Civil Security and Public Safety. *Drones* **2019**, *3*, 59. [CrossRef]
11. Park, K.; Joung, J.; Lim, S.; Lee, H.L. A Compact Crossed Inverted-V Antenna with a Common Reflector for Polarization Diversity in the IoT. *Electronics* **2019**, *8*, 637. [CrossRef]
12. Khang, S.T.; Yu, J.W.; Lee, W.S. Compact folded dipole rectenna with RF-based energy harvesting for IoT smart sensors. *Electron. Lett.* **2015**, *51*, 926–928. [CrossRef]
13. Bhatti, R.A.; Im, Y.T.; Park, S.O. Compact PIFA for mobile terminals supporting multiple cellular and non-cellular standards. *IEEE Trans. Antennas Propag.* **2009**, *57*, 2534–2540. [CrossRef]
14. Saed, M.A.; Yadla, R. Microstrip-fed low profile and compact dielectric resonator antennas. *Prog. Electromagn. Res.* **2006**, *56*, 151–162. [CrossRef]
15. Samsuzzaman, M.D.; IsLam, M.T.; Singh, M.S.J. A Compact Printed Monopole Antenna with Wideband Circular Polarization. *IEEE Access* **2018**, *6*, 54713–54725. [CrossRef]
16. Azadegan, R.; Sarabandi, K. A novel approach for miniaturization of slot antennas. *IEEE Trans. Antennas Propag.* **2003**, *51*, 421–429. [CrossRef]
17. Quan, X.; Li, R.; Cui, Y.; Tentzeris, M.N. Analysis and Design of a Compact Dual-Band Directional Antenna. *IEEE Antennas Wirel. Propag. Lett.* **2012**, *11*, 547–550. [CrossRef]
18. Guo, J.; Zou, Y.; Liu, C. Compact Broadband Crescent Moon-Shape Patch-Pair Antenna. *IEEE Antennas Propag. Mag.* **2011**, *10*, 435–437.
19. Wen, L.H.; Gao, S.; Luo, Q.; Mao, C.X.; Hu, W.; Yin, Y.; Zhou, Y.; Wang, Q. Compact Dual-Polarized Shared-Dipole Antennas for Base Station Applications. *IEEE Trans. Antennas Propag.* **2018**, *66*, 6826–6834. [CrossRef]
20. Wang, M.S.; Zhu, X.Q.; Guo, Y.X.; Wu, W. Compact Circularly Polarized Patch Antenna with Wide Axial-Ratio Beamwidth. *IEEE Antennas Wirel. Propag. Lett.* **2018**, *17*, 714–718. [CrossRef]
21. Wong, H.; So, K.K.; Ng, K.B.; Luk, K.M.; Chan, C.H.; Xue, Q. Virtually shorted patch antenna for circular polarization. *IEEE Antennas Wirel. Propag. Lett.* **2010**, *9*, 1213–1216. [CrossRef]
22. Kim, K.-S.; Kim, G.; Chae, S.-C.; Jo, H.-W.; Yu, J.-W.; Lee, H.L. A Compact Circular Polarization Antenna Using Folded Ground Elements. *IEEE Trans. Antennas Propag.* **2019**, *67*, 3472–3477. [CrossRef]

23. Row, J.S.; Tsai, C.W. Pattern Reconfigurable Antenna Array with Circular Polarization. *IEEE Trans. Antennas Propag.* **2016**, *64*, 1025–1030. [CrossRef]

24. Row, J.S.; Huang, Y.J. Reconfigurable Antenna with Switchable Broadside and Conical Beams and Switchable Linear Polarized Patterns. *IEEE Trans. Antennas Propag.* **2018**, *66*, 3752–3756. [CrossRef]

25. Chen, S.L.; Qin, P.Y.; Lin, W.; Guo, Y.J. Pattern-Reconfigurable Antenna with Five Switchable Beams in Elevation Plane. *IEEE Antennas Wirel. Propag. Lett.* **2018**, *17*, 454–457. [CrossRef]

26. Kim, S.; Yoon, S.; Lee, Y.; Shin, H. A Miniaturized Butler Matrix Based Switched Beamforming Antenna System in a Two-Layer Hybrid Stackup Substrate for 5G Applications. *Electronics* **2019**, *8*, 1232. [CrossRef]

27. Mousavi, Z.; Rezaei, P. Millimetre-wave beam-steering array antenna by emphasising on improvement of Butler matrix features. *IET Microw. Antennas Propag.* **2019**, *13*, 1287–1292. [CrossRef]

28. Trinh-Van, S.; Lee, J.M.; Yang, Y.; Lee, K.-Y.; Hwang, K.C. A Sidelobe-Reduced, Four-Beam Array Antenna Fed by a Modified 4 × 4 Butler Matrix for 5G Applications. *IEEE Trans. Antennas Propag.* **2019**, *67*, 4528–4536. [CrossRef]

29. Cheng, X.; Yao, Y.; Tomura, T.; Hirokawa, J.; Yu, T.; Yu, J.; Chen, X. A Compact Multi-Beam End-Fire Circularly Polarized Septum Antenna Array for Millimeter-Wave Applications. *IEEE Access* **2018**, *6*, 62784–62792. [CrossRef]